Numerical approaches and experimental verification of the conical indentation techniques for residual stress evaluation

Jin Haeng Lee,[a] Hyungyil Lee, Hong Chul Hyun, and Minsoo Kim
Sogang University, Department of Mechanical Engineering, Seoul 121-742, Republic of Korea

(Received 30 March 2010; accepted 7 July 2010)

Conical indentation methods to determine residual stress are proposed by examining the finite element solutions based on the incremental plasticity theory. We first note that hardness depends on the magnitude and sign of residual stress and material properties and can change by up to 20% over a specific range of elastic tensile and compressive residual stress, although some prior indentation studies reported that hardness is hardly affected by residual stress. By analyzing the characteristics of conical indentation, we then select some normalized indentation parameters, which are free from the effect of indenter tip rounding. Adopting dimensional analysis, we present practical conical indentation methods for the evaluation of elastic/plastic equi- and nonequi-biaxial residual stresses. The validity of developed approaches is confirmed by applying them to the experimental evaluation of four-point bending stress.

I. INTRODUCTION

Residual stresses are formed by diverse processes. The residual stresses in materials affect the behavior of materials, including fatigue, fracture, corrosion, abrasion, and friction. For this reason, various experimental measuring techniques have been developed, e.g., neutron and x-ray tilt techniques, strain/curvature measurements, beam bending, hole drilling, layer removal, and chemical etching.[1,2] Each of these methods, however, has a shortcoming with respect to accuracy, sensitivity, resolution, cost, specimen preparation, material type, and geometry of structure. An indentation test is another method that can evaluate residual stresses. It is nondestructive and easy to use; moreover, it can be applied to small specimens and parts in present structural use. To evaluate residual stresses using an indentation test, it is necessary to secure the indentation data at the non-residual state.

In the first stage, attention was focused on the variation of hardness with the direction and magnitude of residual stresses. Tsui et al.[3] and Bolshakov et al.[4] investigated the effects of residual stresses on hardness, contact area, and elastic modulus using experimental work and finite element analyses (FEA). They showed that residual stress was not related to material hardness but closely to the pileup of material. On the assumption that material hardness is independent of triaxial stress, Suresh and Giannakopoulos (SG)[1] suggested a novel methodology to determine surface equi-biaxial residual stress with sharp indentation, invoking the invariance of contact pressure (or hardness). For a given residual stress σ_R, they assumed the following relation,

$$P^{o}_{max} = P_{max} + \sigma_R f_c A \quad , \qquad (1)$$

where P_{max} and P^{o}_{max} are the maximum loads at the same indentation depth h_{max} with and without residual stress, respectively. A is the projected contact area for the material with residual stress after unloading (Fig. 1). It should be noted that although some indentation studies use the contact area at the maximum load to measure elastic modulus, hardness, etc., we use the contact area after unloading because it is the only parameter we can measure from indentation tests. In addition, the hardness invariant assumption of the SG method is based on Tsui et al.'s experimental work.[3] They used measured contact area, which is obviously the area after unloading, and found that the hardness is almost independent of residual stress. Therefore, it is sufficiently and more meaningful to use the area after unloading in this study. Geometric factor f_c in Eq. (1) is 1 for tensile residual stress and $\sin\alpha$ for compressive residual stress, where $\alpha = \pi/2 - \theta$ as shown in Fig. 1. Suresh and Giannakopoulos[1] introduced geometric factor since, unlike the tensile residual stress, compressive residual stress acts counter to the direction of the indentation load. For Vickers indentation, the geometric factor of SG is around 0.375. By modifying the SG's method, Lee and Kwon[5] decomposed equi-biaxial residual stress into mean and deviatoric stresses, and then they assumed that only the parallel component of deviatoric stress to the direction of indentation is related to plastic deformation. The geometric factor f_c of Lee and

[a]Address all correspondence to this author.
e-mail: jinhaeng@sogang.ac.kr
Present address: Korea Atomic Energy Research Institute, Yuseong-gu, Daejeon 305-353, Republic of Korea.
DOI: 10.1557/JMR.2010.0275

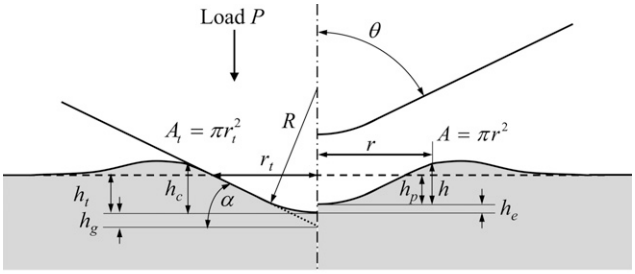

FIG. 1. Schematic of sharp indentation profiles considering tip-rounding effect.

Kwon[5] is around 0.667. On the other hand, Atar et al.[6] illustrated that the geometric factor in ceramic thin films should be unity by comparing residual stresses from indentation tests with those determined by x-ray diffraction (XRD) for compressive residual stress. In fact, it cannot be physically justified to distinguish between tensile and compressive residual stresses.

Xu and Li[7] investigated the unloading behavior in nanoindentation under equi-biaxial residual stress state by finite element (FE) simulations and demonstrated that the residual stress has a slight effect on the hardness. However, they did not provide any quantitative expression of residual stresses in terms of indentation parameters on the basis of their investigation. Chen et al.[8] proposed a numerical method to simultaneously determine elastic modulus, yield strength, and residual stress through one simple indentation test. They obviously showed that hardness depends on residual stress. Their method is useful because it does not require a reference stress-free material for comparison purposes. However, they did not mention the effect of strain-hardening exponent to which the method can be very sensitive.

Most of the previously mentioned studies missed out the effects of material properties, friction coefficient, or indenter tip radius on the evaluation of residual stress. The finite tip radius caused by a manufacturing problem and wear are inevitable. For the same contact area, if their tip radii are different, the measured indentation depth varies from one indenter to the other.[9] This causes some trouble in transferring the information obtained from one indenter to the other with a different tip radius. Thus, prior studies on the evaluation of residual stress are not yet fully validated for general materials and indenters with tip rounding. The present work deals with these issues, which have been easily ignored in the previous works, via FE approaches and experimental verification of conical indentation techniques for residual stress evaluation.

The paper is organized as follows. In Sec. II, we investigate the relation between residual stress and indentation parameters. We present two methods for evaluating elastic/plastic residual stress based on FE solutions using the incremental theory of plasticity in Sec. III. From the actual indentation tests, we measure 4-point linearly varied elastic bending stresses, and discuss the reliability of the method to evaluate biaxial residual stress in Sec. IV. Finally, some conclusions are given in Sec. V.

II. FINITE ELEMENT MODELING AND ANALYSIS

A. FE modeling of indentation tests

We performed nonlinear geometry change FE analyses using isotropic elasto–plastic material, which obeys the J_2 flow theory. Considering both loading and geometric symmetry, we used the four-node axisymmetric element CAX4.[10] Our previous work[11] revealed that the eight-node CAX8 element in ABAQUS[10] has the problem of discontinuous equivalent plastic strain at its mid-node. The lower degree of CAX4 shape function is supplemented by placing fine elements of which size, e, is 0.625% of the maximum indention depth at the material contact surface. Multipoint constraints (MPC) option is conveniently used at the transition region where element size changes. However, constrained mid-nodes of MPC tend to give discrete stress and strain values. We thus adopted trapezoidal elements in the transition region near the contact surface and used MPC in the transition region far from the contact surface. The FE model consists of about 18,000 elements. We also placed contact surfaces on both material and indenter surfaces. Coulomb friction coefficient f is selected as 0.3. Section II. B deals with the effects of f. Axisymmetric boundary conditions are imposed on the nodes on the axisymmetric axis. The rigid conical indenter with a rounded tip moves down to indent the material specimen with its bottom fixed. This FE model is basically the same as our previous work[9] except for the rigid indenter in the present work. Self-similar indenters with an ideally sharp tip such as a cone, Berkovich and Vickers obey Kick's law $P = Ch_t^2$.[1,12] The finite tip radius R (>0) inevitable in reality may defy the self-similarity. However, the effect of tip radius R on indentation tests can be minimized by means of appropriate normalized parameters.[9] The gap h_g of indentation depth between perfect and rounded tips is given in the form (Fig. 1)

$$h_g = R\left(\frac{1}{\sin\theta} - 1\right) \quad , \tag{2}$$

where θ is the half-included tip angle of the conical indenter. In this study, θ and R/h_{max} are fixed as 70.3° and 2, respectively.

Table I shows the representative material properties of piecewise power law[13] in Eq. (3) used for FE analyses. It is noteworthy that these values comprehensively cover the property range of general metals.

TABLE I. Material properties used in FE indentation analysis.

Material property	Values used in FEA
Young's modulus E (GPa)	100, 200
Yield strain ε_o	0.001, 0.002, 0.003, 0.004, 0.006, 0.008, 0.01
Strain-hardening exponent n	1.5, 2, 3, 5, 7, 10, 20

$$\frac{\varepsilon_t}{\varepsilon_o} = \begin{cases} \dfrac{\sigma}{\sigma_o} & \text{for} \quad \sigma \le \sigma_o \\ \left(\dfrac{\sigma}{\sigma_o}\right)^n & \text{for} \quad \sigma > \sigma_o; 1 < n \le \infty \end{cases}, \qquad (3)$$

where σ_o is yield strength, ε_o is yield strain, and n is the strain-hardening exponent. Total strain ε_t is decomposed into elastic and plastic strains ($\varepsilon_t = \varepsilon_e + \varepsilon_p$). To preset the state of equi-biaxial residual stress in the FE model, we studied two kinds of methods. One is the initial boundary condition method done by imposing initial prescribed radial displacements at the outer boundary of the FE model. The other is the initial stress method done by using the ABAQUS option.[10] To use initial stress option, the radial displacement at the outer boundary must be fixed as a zero value. We have confirmed that they produce identical results. In this work, we use initial stress option since it is easier than the boundary condition method in imposing residual stresses on the FE mesh.

B. Effects of Coulomb friction coefficient

The friction force arises from the interaction of the surface layers of the bodies. The friction coefficient f of the Coulomb friction model varies with materials and lubrication. We observe that the friction coefficient does not change the load–depth (P–h_t) curve regardless of material properties and the sign of residual stress. Figure 2 shows the effect of friction on hardness H ($\equiv P_{max}/A$) and contact area A after unloading (Fig. 1) for various residual stresses. A_t in Fig. 2(b) means ideal contact area at loaded state without considering pileup/sink-in effect, $A_t = \pi\,[(h_{max} + h_g)\tan\theta\,]^2$ (Fig. 1). Unlike the load–depth curve, hardness is partially affected by friction coefficient [Fig. 2(a)], especially for materials with a large strain-hardening exponent. That friction coefficient changes the contact area [Fig. 2(b)], while it hardly changes the load. These results are similar to those of spherical indentation.[11,14,15] Because the friction effect increases with contact area (or pileup) that also increases with strain-hardening exponent at the same yield strain ε_o, the effect of friction coefficient on contact area [Fig. 2(b)] increases with strain-hardening exponent.

On the assumption that material hardness is independent of triaxial stress, SG[1] proposed a method evaluating equi-biaxial residual stress. Their basic Eq. (1) for $f_c = 1$ can be rewritten as

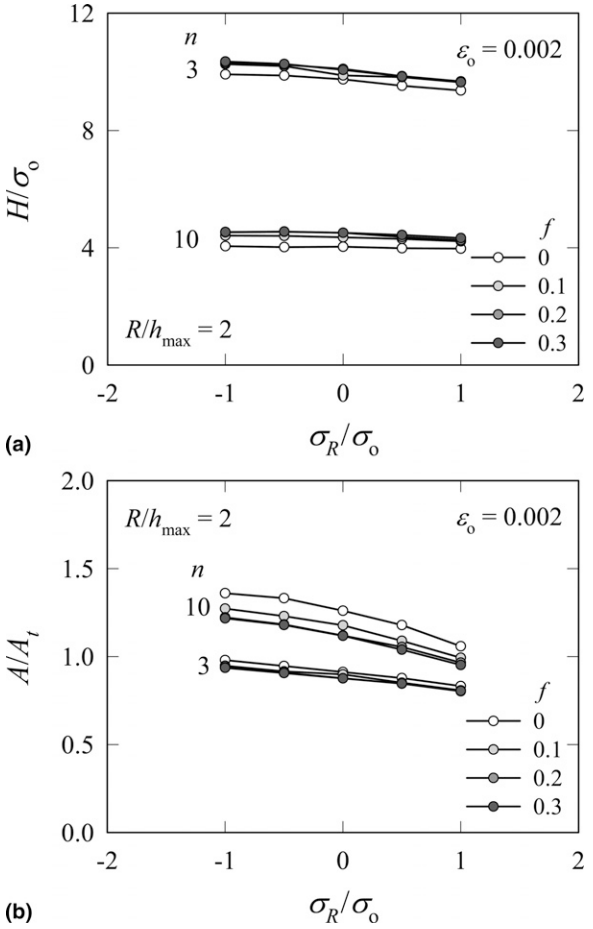

FIG. 2. Influence of friction coefficients on (a) hardness–residual stress curves and (b) A/A_t–residual stress curves.

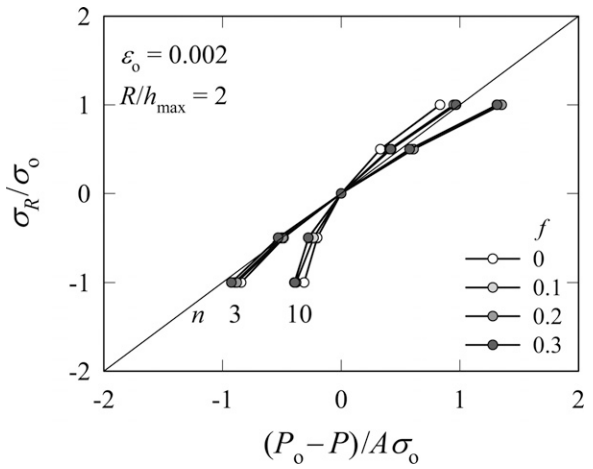

FIG. 3. Effect of friction coefficients on given σ_R versus predicted σ_R curves.

$$\sigma_R = \frac{(P^o_{max} - P_{max})}{A} \quad . \qquad (4)$$

Figure 3 compares the residual stresses predicted by Eq. (4) as $(P^o_{max} - P_{max})/(A\sigma_o)$ with those given (σ_R/σ_o)

for four values of f. Predicted residual stresses vary with f as Eq. (4) includes indentation contact area. The tendency increases with strain-hardening exponent. Contrary to many prior studies using the frictionless contact condition, however, the deviation of the indentation parameters between $f > 0$ and $f = 0$ is not negligible as shown in Figs. 2 and 3. Note that the frictional effect is very small once $f > 0.1$.

Figure 3 also reveals that the accuracy of residual stress predicted by Eq. (4) depends on the strain-hardening exponent. We probe the effect of material properties on the evaluation of residual stress in Sec. II. C.

C. Verification of prior indentation theories

The variation of hardness with residual stress for various material properties is presented in Fig. 4(a). Here, H_o is hardness under residual stress-free condition. It should be noted that when the absolute value of a σ_R is greater than σ_o in Fig. 4(a), plastic deformation caused by plastic residual stress pre-exists. Hence, it can be considered that the comparison with the hardnesses under plastic residual stress state is meaningless, as shown in Fig. 4(a), since the reference hardness work-hardened by plastic residual stress is not the same as that of residual stress-free state, H_o. It is, however, often unrealistic to measure hardness after removing residual stress in actual structures, therefore it is more practical to set the reference hardness as the original value under the residual stress-free condition, regardless of the elastic/plastic residual stress state. Hence, this comparison will give valuable information about the difference between elastic and plastic residual stress states.

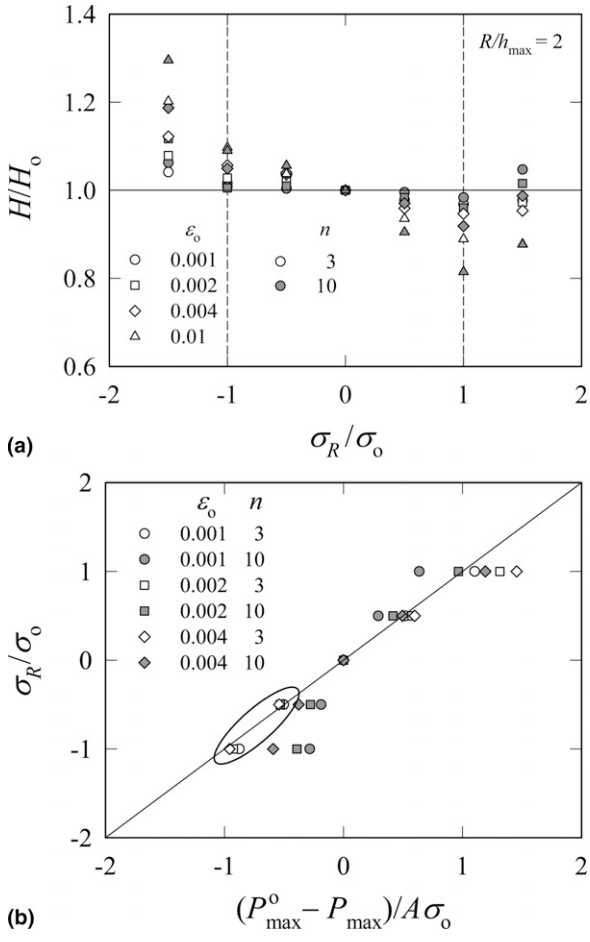

FIG. 4. (a) Normalized hardness H/H_o versus σ_R/σ_o and (b) σ_R/σ_o versus the ratio between load deviation and contact area A computed using Eq. (4) for various material properties.

It is clarified in Fig. 4(a) that hardness depends on the residual stress and material properties, even though elastic residual stress state is assumed, while some prior indentation studies[1,3,4] reported and assumed that hardness is hardly affected by residual stress. These prior studies were limited to a narrow range of materials with little thought of various materials. Xu and Li[7] and Chen et al.,[8] who have used finite element analysis, have found hardness variation, and especially Chen et al. have obviously shown that hardness was greatly affected by σ_o/E ratio for elastic–perfectly plastic materials. In their study, when $\sigma_R/\sigma_o = 1$ and $\sigma_o/E = 0.01$, the hardness decreases by 20% of reference hardness for an elastic–perfectly plastic material, and our study shows a similar amount of hardness drop for a similar condition ($\sigma_R/\sigma_o = 1$, $\sigma_o/E = 0.01$, and $n = 10$), as shown in Fig. 4(a). Consequently, significant errors in the predicted value of residual stress are unavoidable (especially high σ_o/E materials) when we use the formula based on an assumption of hardness invariance.

In Fig. 4(a), it should also be noted that hardness can increase with applied tensile residual stress when $\sigma_R/\sigma_o > 1$, whereas it always decreases with increasing elastic tensile residual stress. This is because for a fixed indentation depth, the contact area continuously decreases with increasing tensile residual stress regardless of the magnitude of the tensile residual stress, but the indentation load, which has also decreased with increasing applied tensile residual stress, can increase with residual stress when $\sigma_R/\sigma_o > 1$. This means that we could not distinguish plastic residual stress from elastic residual stress when the indentation load deviation is only considered; the contact area or other parameters equivalent to contact area should be included for plastic residual stress evaluation.

For relatively σ_o/E high ratio ($\sim$0.1), even in the elastic compressive residual stress state the turnover of hardness can be found,[8] but noting that σ_o/E values of most metallic materials are smaller than 0.1, in this work we will not deal with this phenomenon.

Figure 4(b) compares the elastic residual stresses predicted by Eq. (4) as $(P^o_{max} - P_{max})/(A\sigma_o)$ with those given σ_R/σ_o for various materials. The figure reveals that predicted residual stress depends on material properties,

especially the error of predicted residual stress increases with strain-hardening exponent n. For compressive residual stress, SG calculated residual stress by Eq. (1) with $f_c = \sin\alpha$, but use of $\sin\alpha$ does not reduce the scattering. If $n = 3$ for compressive residual stress in Fig. 4(b) (open symbols in the ellipse), the geometric factor f_c should be rather unity than $\sin\alpha$. This is because SG suggested Eq. (1) by studying only aluminum 8009 material ($\varepsilon_o = 0.0043$, $n \approx 12$).

Another issue with Eq. (4) is that it omits the effects of variations of contact area. If hardness is independent of residual stress, contact area at the same indentation load should not be changed by residual stress. Figure 5 shows the deformed geometries for a material under three different indentation conditions. Figures 5(a) and 5(b) are residual stress-free states with different indentation depths, and Fig. 5(c) is a compressive residual stress state. Their indentation loads are P_1, P_2, P_3, and contact areas are A_1, A_2, A_3, respectively. We set the contact areas $A_2 = A_3 > A_1$ and indentation depths $h_2 = h_3 > h_1$. If we assume hardness invariance, the hardness of Figs. 5(a)–5(c) should be identical, that is, $P_2 = P_3 > P_1$. This can be understood to mean that the differential load ($P_3 - P_1$) is exclusively caused by the variation of A under hardness invariance assumption. SG's differential load is, however, produced by hydrostatic stress, and their theory using the fixed boundary layer does not express the effect of area deviation. Consequently, Eq. (4) is insufficient to represent the invariance of hardness and the effect of hydrostatic stress simultaneously and, moreover, the hardness invariance assumption is untrue [Fig. 4(a)].

As demonstrated above, both hardness and measured residual stress by Eq. (4) depend on the magnitude and sign of residual stress and material properties. It should be noted that when $\varepsilon_o = 0.01$ and $n = 10$, the error of estimated residual stress is over $\pm 30\%$, whereas the hardness change is just up to $\pm 5\%$. Even if we decrease the R/h_{max} ratio, we obtain the same trend. To explain the real indentation phenomenon, it needs a new indentation model, including variation of contact area. The main reason why hardness looks invariant is that actual mean indentation depth h_m decreases with increasing pileup. Here, h_m is defined as the value of the indented (or compressed) volume V divided by projected contact area A. Considering that the ideal volume of cone V_t is $A_t h_t/3$, ideal mean indentation depth h_{tm} is $h_t/3$. In pileup, the vertical direction of displacement at the contact edge is opposite the indentation direction, so actual mean indentation depth is lower than the ideal mean indentation depth. In sink-in, additional displacement ($h_t - h_c$) occurs where h_c is the actual indentation depth (Fig. 1), so actual mean indentation depth is higher than ideal depth. We can thus express actual mean indentation depth h_m in the form

$$h_m = h_t - \frac{2}{3} h_c \quad . \tag{5}$$

In indentation tests, contact area (or actual contact indentation depth h_c) increases with magnitude of compressive residual stress. Load increment due to compressive residual stress and increment of contact area is offset by load decrement due to decrement in actual mean indentation depth, and hardness might seem to be hardly affected by residual stress for specific materials. But obviously, hardness varies with the magnitude and sign of residual stress and material properties as shown in Fig. 4(a) because indentation geometries are quite different for the same material with and without residual stress at the same contact area (Fig. 5). Hence, the assumption of hardness invariance has no physical basis.

III. NUMERICAL APPROACHES TO EVALUATE RESIDUAL STRESS

A. A numerical approach using contact area for evaluation of elastic/plastic residual stress

In Sec. II, we have confirmed that hardness varies largely with the magnitude and sign of residual stress and material properties. In this section, a new method to evaluate elastic/plastic residual stress considering the effect of material characteristics on residual stress evaluation is proposed on the basis of FEA solutions.

Xu and Li[7] showed that the relationship between A/A_t and σ_R/σ_o depends on material properties. Here, A is actual projected contact area and A_t is ideal contact area (Fig. 1), and σ_R/σ_o is the residual stress normalized by yield strength. As explained in Sec. I, we use the contact area after unloading in this study. Figure 6(a) demonstrates that the ratio A/A_t is a meaningful parameter in the evaluation of residual stress by indentation. The ratio of predicted stress to imposed residual stress

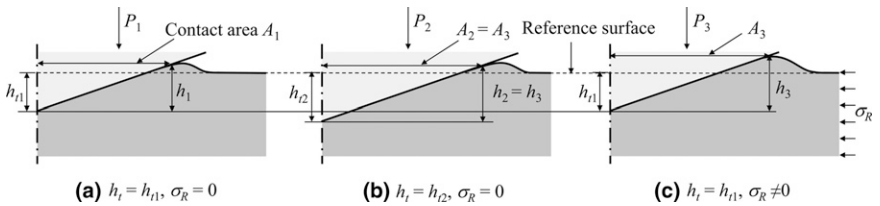

FIG. 5. The geometries for three indentation conditions with different indentation depth and residual stress.

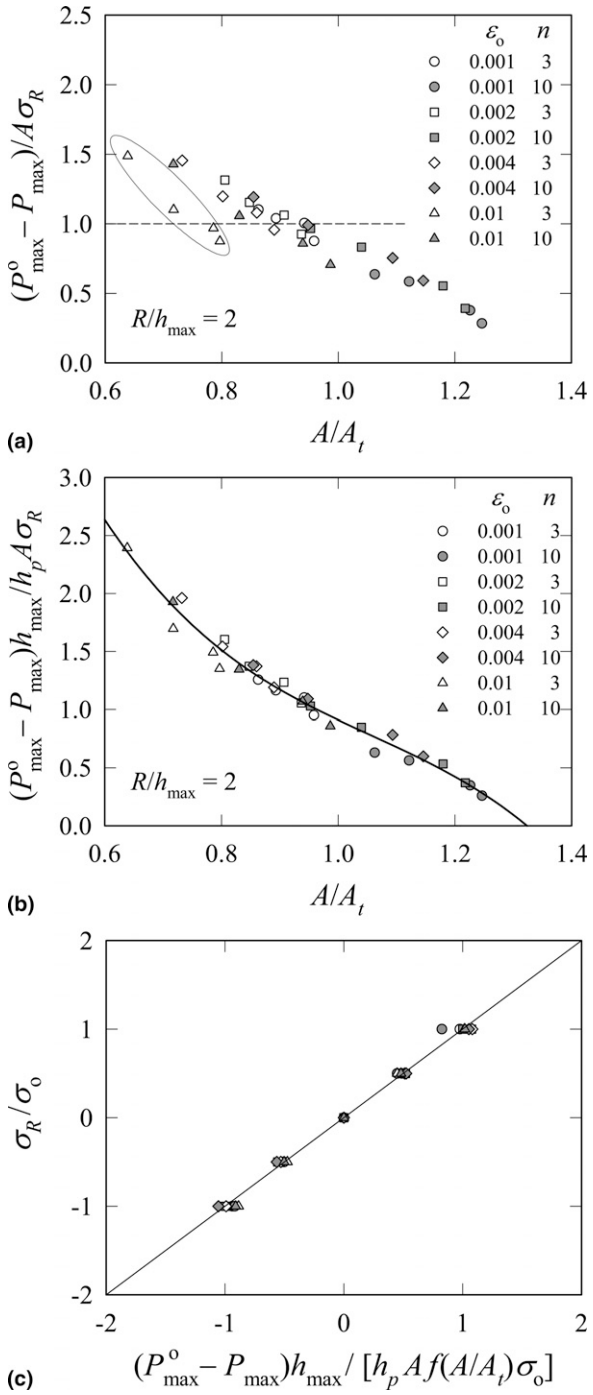

FIG. 6. (a) Normalized indentation parameter $(P^o_{max} - P_{max})/A\sigma_R$ versus the ratio between actual and ideal indentation area A/A_t and (b) normalized indentation parameter considering elastic recovery $(P^o_{max} - P_{max})h_{max}/h_pA\sigma_R$ versus the ratio between actual and ideal indentation area A/A_t. (c) Imposed residual stress versus predicted residual stress considering elastic recovery and ideal contact area A for various material properties.

$[(P^o_{max} - P_{max})/(A\sigma_R)]$ is not unity, except for $A/A_t = 0.9$ region, and increases with decreasing A/A_t. Pileup/sink-in changes contact area, mean indentation depth, and subindenter constraint in a rather consistent manner, except for the material with yield strain $\varepsilon_o = 0.01$ and strain-hardening exponent $n = 3$ in Fig. 6(a) (open triangles in the ellipse).

Suresh and Giannakopoulos[1] claimed that hardness is almost independent of residual stress if the elastic strains are much smaller than the plastic strains ($\varepsilon_o < 0.007$). Provided that the elastic deformation of material is independent of residual stress,[1] the ratio of plastic strain to total strain plays an essential role in exact residual stress evaluation for a wide range of materials. Hence, plastic indentation depth h_p after unloading, which can be obtained from the indentation load–depth curve, is another meaningful parameter. Figure 6(b) reveals that the parameter with the depth ratio (h_{max}/h_p) gives a narrow band for all materials, including the material with large elastic recovery ($\varepsilon_o = 0.01$ and $n = 3$). With the solid line [$= f(A/A_t)$], which is the third order polynomial regression of the data in Fig. 6(b), we express residual stress in the form:

$$\sigma_R = \frac{(P^o_{max} - P_{max})h_{max}}{Ah_p f(A/A_t)} \quad . \tag{6}$$

Equation (6) provides residual stress with an average and maximum error of less than 5% and 25%, respectively, for all kinds of metal [Fig. 6(c)]. To use this method, we must measure contact areas A after unloading and A_t (or R).

B. A numerical approach using material properties for evaluation of elastic residual stress

Equation (6) using load, depth, and contact area to evaluate equi-biaxial residual stresses has a somewhat limited practicality because it requires measuring or predicting the projected contact area A after unloading. Material properties can be known or obtained from the test such as spherical indentation.[11,15] In such a case, we can estimate elastic residual stress in a rather simple way without using contact area A since the effects of pileup/sink-in can be merged into material properties.[11]

Kick's law gives the relationship of load–depth curve:

$$P = C(h_t + h_g)^2 \quad . \tag{7}$$

The gap of indentation depth between perfect and rounded tips h_g is given as in Eq. (2). The tip radius R invalidates Eq. (7) at the initial stage of indentation, but the validity increases with indentation depth h_t. Lee et al.[9] have shown that C converges if $h_{min}/h_{max} > 0.5$ where h_{min} is the lower limit depth of the regression. Use of C instead of P allows us to be free from the tip-radius effect. Another conceivable advantage of Eq. (7) is that it can also additively include the effect of initial penetration depth h_i due to the initial contact force needed to make actual contact initially.[16] Kick's law, including initial

penetration depth h_i (> 0), can be expressed in its final modified form:

$$P = C(h_t + h_g + h_i)^2 \quad . \tag{8}$$

In the present FEA work, initial penetration depth $h_i = 0$, therefore we use Eq. (7). In actual indentation tests, Eq. (8) is more appropriate.

Considering that C has the dimension of stress, we suggest this formula for equi-biaxial residual stress:

$$\frac{\sigma_R}{\sigma_o} = f\left(\frac{C_o - C}{\sigma_o}, \varepsilon_o, n\right) \quad , \tag{9}$$

where semimaterial constant C_o for residual stress-free state and constant C for nonzero residual stress state can be obtained from the regression of load–depth curve between $0.5h_{max}$ and h_{max}. We performed FE analyses of a total of 245 cases (residual stress: 5 × yield strain: 7 × strain-hardening exponent: 7), and obtained the values of regression constant C of Eq. (7) for 245 cases. The FE solutions can be expressed with the following polynomial formula:

$$\frac{\sigma_R}{\sigma_o} = f_i^{\sigma_R}(\varepsilon_o, n)\left(\frac{C_o - C}{\sigma_o}\right)^i \quad , \tag{10}$$

$$f_i^{\sigma_R}(\varepsilon_o, n) = \alpha_{ij}(\varepsilon_o) n^{-j}; \quad i = 1,2, j = 0,1,2,3,4 \quad ,$$

$$\alpha_{ij}(\varepsilon_o) = \beta_{ijk}\varepsilon_o^k; k = 0,1,2,3(\text{Appendix}) \quad .$$

The values of coefficients of Eq. (10) are given in the Appendix (Table AI).

Figure 7 compares predicted residual stresses with real residual stresses for various material properties. Equation (10) provides residual stress with an average error of less than 3% for all kinds of metal. This approach is truly convenient when material properties can be readily obtained in advance because it does not measure actual contact area A. We confirmed that Eq. (10) is also valid for other low ratios of R/h_{max} (0.5 and 1) and a deformable diamond indenter ($E = 1000$ GPa and $\nu = 0.1$).

For additional convenience, on the assumption that material can be described well with two parameter fitting, we expressed the values of C_o for residual stress-free state as a function of material properties as follows:

$$\frac{C_o}{E} = f_i^C(\varepsilon_o) n^{-i} \quad , \tag{11}$$

$$f_i^C(\varepsilon_o) = \gamma_{ij}\varepsilon_o^j; i = 0,1,2,3 j = 0,1,2,3(\text{Appendix}) \quad .$$

The values of coefficients of Eq. (11) are given in the Appendix (Table AII). In a case where the stress–strain curve can be well expressed by the power law fitting, Eq. (11) makes Eq. (10) simple and useful to evaluate equi-biaxial residual stress since a reference stress-free material as measuring C_o is not required.

Note that by using no load P but the coefficient C, we can suppress numerous errors caused by friction and tip radius. As shown in Sec. II. B, the friction coefficient

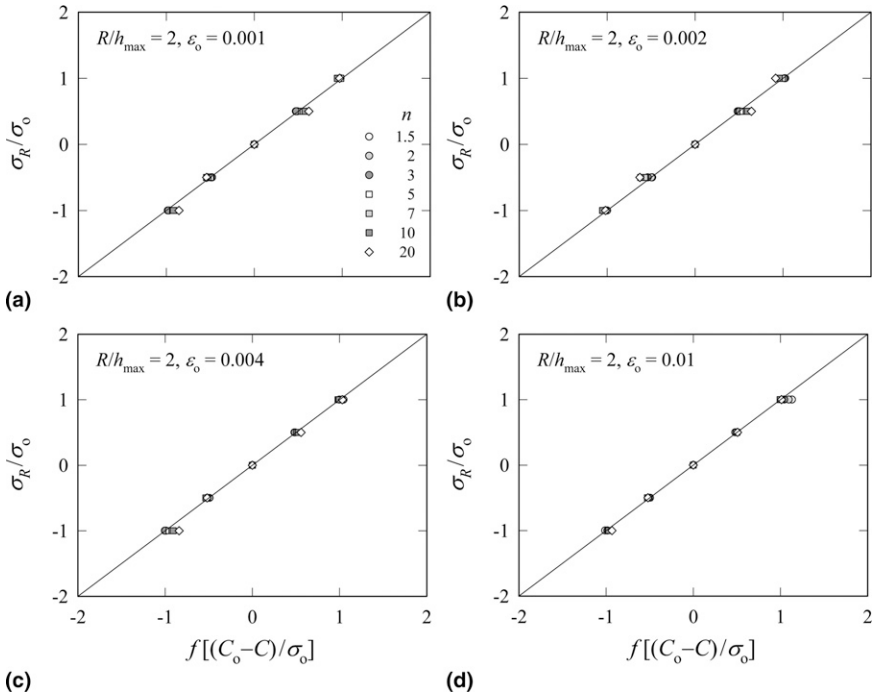

FIG. 7. Comparison of residual stress versus indentation parameter for (a) $\varepsilon_o = 0.001$, (b) 0.002, (c) 0.004, and (d) 0.01.

hardly changes the indentation load (and C) while it changes the contact area. Furthermore, as we simply use the deviation of coefficients C, the frictional effect is almost self-eliminated. It is important to reduce tip-radius effect by using regression forms of Eqs. (7) and (8), because it means we can drastically reduce the maximum indentation load (or depth) for a given indenter tip without measuring its radius, and therefore can easily increase indentation points to improve the resolution of residual stress distribution.

C. Estimation of general elastic biaxial residual stresses using material properties

Residual stress states are not generally equi-biaxial. In such cases, it is hard to evaluate general nonequi-biaxial residual stresses by conical, Berkovich, Vickers, and spherical indenters because we cannot observe the difference of the load–depth curves, regardless of the alignment of orientations between indenter and specimen. On the presumption that the ratio of biaxial residual stresses is known, Lee and Kwon[5] suggested a method to evaluate general biaxial residual stresses with sharp indenters by the relation:

$$\sigma_{R2} = \frac{3(P^{o}_{max} - P_{max})}{(1+\kappa)A} \quad , \tag{12}$$

where κ is the ratio of biaxial residual stresses, σ_{R1}/σ_{R2}. The relation is useful when either uniaxial residual stress state is assumed or the ratio of biaxial residual stresses is known, but Eq. (12) is also inherently based on SG's method. It should be noted that the residual stress increment is generally not proportional to the load decrement, as demonstrated by the above FEA solutions for various material properties. To examine the characteristics of load–depth distribution at general nonequi-biaxial residual stress states, we generated three-dimensional (3D) FE models for Berkovich and conical indentations. Symmetry in geometry and loading allows modeling a half for Berkovich and a quarter for conical indenters. We compared load–depth curves with element type and indenter geometry for a specific equi-residual stress state. Two load–depth curves of 3D Berkovich and cone models coincide well with that of a two-dimensional axisymmetric model, but further study is needed to generalize the relationship between conical and Berkovich indenters since the relationship depends on material properties. For elastic materials, a Berkovich indenter gives a relatively higher maximum load than an equivalent conical indenter at the same indentation depth.[17,18] Elastic–plastic materials, including large elastic deformation, i.e., large yield strain or small strain-hardening exponent materials, thus show load deviation between conical and Berkovich indenters.[19,20] In this work, we adopted the conical 3D model in subsequent analyses to estimate general biaxial residual stresses since we used the conical indenter for equi-biaxial residual stress analyses. Figure 8 reveals remarkable features. Maximum load (P_{max}) for nonequi-biaxial residual stress is related to those of equi-biaxial residual stress states. P_{max} for $(\sigma_{R1}, \sigma_{R2}) = (-200, 0)$ nonequi-residual stress state is virtually mean P_{max} of equi-biaxial $(-200, -200)$ and $(0, 0)$ states. P_{max} for $(-400, 0)$ is nearly mean P_{max} of $(-400, -400)$ and $(0, 0)$. P_{max} for $(-400, -200)$ is almost mean P_{max} of $(-400, -400)$ and $(-200, -200)$. On this observation, we propose a procedure to evaluate nonequi-biaxial residual stress if the ratio of residual stress components κ is known.

When the uniaxial residual stress state ($\sigma_{R1} \neq 0$, $\sigma_{R2} = 0$) is assumed, we can estimate it from virtual equi-biaxial residual stress. Using the measured Kick's law coefficient ${}^{Uni}C$ at the uniaxial residual stress state, we have the next expression:

$${}^{Uni}C = \frac{{}^{Equi}C + C_o}{2} \quad , \tag{13}$$

where ${}^{Equi}C$ is Kick's law coefficient when equi-biaxial residual stress σ_{R1} ($= \sigma_{R2}$) acts. Equation (13) can be rewritten as ${}^{Equi}C = 2 \cdot {}^{Uni}C - C_o$.

Using estimated ${}^{Equi}C$, we can obtain the uniaxial residual stress σ_{R1} from Eq. (10).

$$\frac{\sigma_{R1}}{\sigma_o} = f\left(\frac{C_o - {}^{Equi}C}{\sigma_o}, \varepsilon_o, n\right) \quad . \tag{14}$$

If we know the ratio of nonequi-biaxial residual stress, $\kappa = \sigma_{R1}/\sigma_{R2}$ ($\sigma_{R1} \neq \sigma_{R2}$, $\sigma_{R1} \neq 0$, and $\sigma_{R2} \neq 0$), we can also estimate them. Kick's law coefficient ${}^{Bi}C$ at biaxial residual stress state obtained from the indentation test is converted into two virtual equi-biaxial residual stresses. For this conversion, we suppose the next expression:

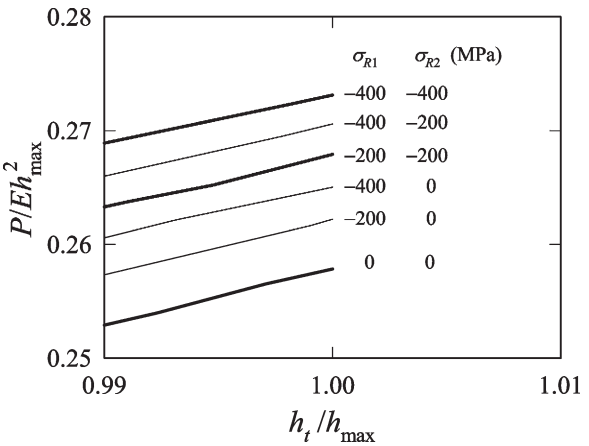

FIG. 8. The distribution of load–depth curves for various equi- and nonequi-biaxial residual stresses.

$$ {}^{\mathrm{Bi}}C = \frac{{}^{\mathrm{Equi}}C_1 + {}^{\mathrm{Equi}}C_2}{2} \quad . \tag{15} $$

${}^{\mathrm{Equi}}C_1$, ${}^{\mathrm{Equi}}C_2$ are virtual Kick's law coefficients when equi-biaxial residual stresses σ_{R1} ($= \sigma_{R2}$), σ_{R2} ($= \sigma_{R1}$) act, respectively. We decompose the measured ${}^{\mathrm{Bi}}C$ into two coefficients ${}^{\mathrm{Equi}}C_1$ and ${}^{\mathrm{Equi}}C_2$ at equi-biaxial residual stress states. If ${}^{\mathrm{Equi}}C_1$ or ${}^{\mathrm{Equi}}C_2$ is C_o in Eq. (15), i.e., uniaxial residual stress state is assumed, ${}^{\mathrm{Bi}}C$ becomes ${}^{\mathrm{Uni}}C$, and Eq. (13) and Eq. (15) are identical. In a uniaxial residual stress state, we estimate residual stress without iteration as we can measure or estimate C_o. In a general biaxial residual stress state, however, we use the iterative method to estimate residual stresses. We first let measured value ${}^{\mathrm{Bi}}C$ be the initial value ${}^{\mathrm{Equi}}_{0}C_1$, and add small variation ΔC to ${}^{\mathrm{Equi}}_{0}C_1$, then calculate ${}^{\mathrm{Equi}}_{1}C_2$ from Eq. (15) as follows:

$$ \begin{aligned} {}^{\mathrm{Equi}}_{1}C_1 &= {}^{\mathrm{Equi}}_{0}C_1 + \Delta C \\ {}^{\mathrm{Equi}}_{1}C_2 &= 2^{\mathrm{Bi}}C - {}^{\mathrm{Equi}}_{1}C_1 \quad . \end{aligned} \tag{16} $$

Substituting ${}^{\mathrm{Equi}}_{1}C_1$, ${}^{\mathrm{Equi}}_{1}C_2$ calculated from Eq. (16) into Eq. (10), we estimate residual stresses ${}_1\sigma_{R1}$ and ${}_1\sigma_{R2}$, respectively. We repeatedly calculate them until the error between ${}_1\sigma_{R1}/{}_1\sigma_{R2}$ and κ converges within the tolerance limit. Figure 9 shows the flow chart for determination of biaxial residual stresses. Table II compares the predicted with actual biaxial residual stresses for some cases.

IV. EXPERIMENTAL VERIFICATION

The material chosen for the study was JIS SS400 (structural steel), which had been annealed at 780 °C to remove residual stresses. The material properties obtained from tensile test using the same specimen were elastic modulus $E = 205$ GPa, yield strength $\sigma_o = 290$ GPa, and Poisson's ratio $\nu = 0.3$.[21]

The indentation tests with the same material were conducted using our microindenter DKTT-3000 system [Fig. 10(a)]. To impose linearly varied uniaxial residual stresses on the specimen, we made a 4-point bending jig as shown in Fig. 10(b). The gaps of inner and outer loading points were 30 and 185 mm, respectively. We mounted two strain gauges on the centerline of the top and bottom surfaces of the specimen. Considering the difference between pyramidal and conical indenters,[17–20] we manufactured a 70.3° tungsten carbide conical indenter for the consistency with FE analysis. Four indentations were made on the unstressed specimen with indentation depth 0.2 mm, and these four curves were almost identical, so that we chose one of them as a reference load–depth data. We then imposed uniaxial elastic residual stresses on the specimen by the 4-point

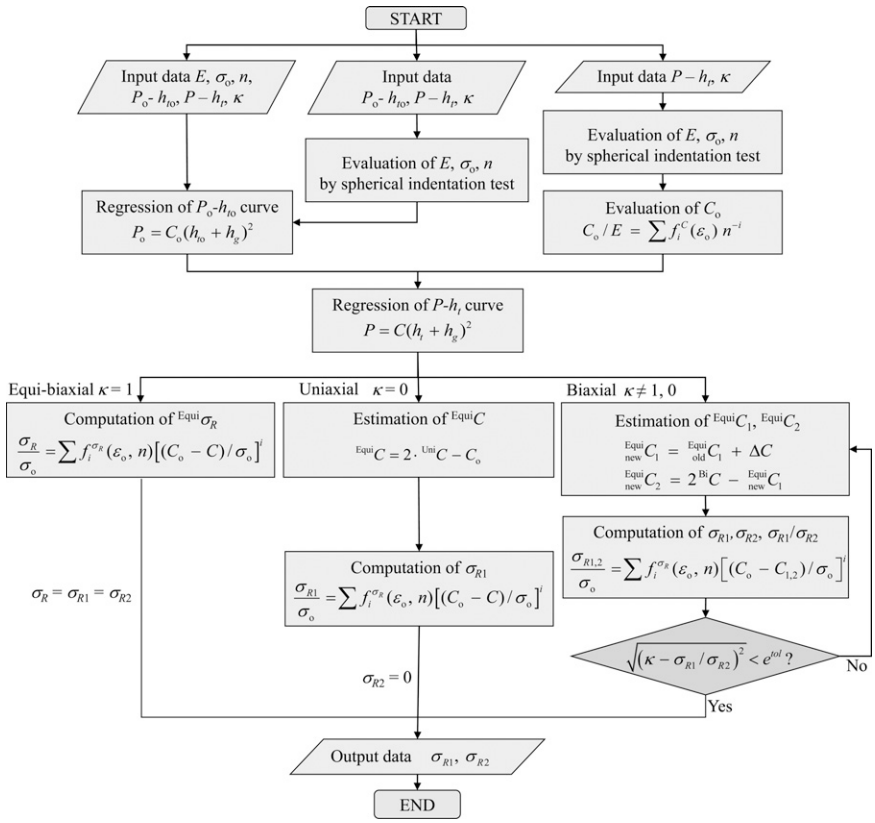

FIG. 9. Flow chart for determination of residual stresses.

TABLE II. Comparison of computed residual stresses to those given.

$\sigma_o = 400$ MPa, $E = 200$ GPa, $n = 3$				
σ_{R1} (MPa)	σ_{R2} (MPa)	Predicted σ_{R1} (MPa)	Predicted σ_{R2} (MPa)	Error (%)
−400	0	−346	0	13
−400	−200	−385	−193	3.8
−400	−400	−377	−377	5.8
400	0	419	0	4.8
400	200	395	198	1.3
400	400	373	373	6.8
$\sigma_o = 400$ MPa, $E = 200$ GPa, $n = 10$				
σ_{R1} (MPa)	σ_{R2} (MPa)	Predicted σ_{R1} (MPa)	Predicted σ_{R2} (MPa)	Error (%)
−200	0	−173	0	13
−400	0	−332	0	17
−200	−200	−189	−189	5.5
−400	−400	−382	−382	4.5
200	0	200	0	0.1
400	0	424	0	6.0
200	200	188	188	6.0
400	400	361	361	9.8

bending, and selected 15 positions (3 columns × 5 rows) on the surface spread with the column and row intervals of 7.5 and 6 mm. The reference and five stressed load–depth curves obtained from center column are shown in Fig. 11. Note that the surface roughness is a very important factor in nanoindentation tests, but it is not a critical issue on microindentation tests. The maximum indentation depth is 0.2 mm, which is large enough to neglect the effect of surface roughness on the residual stress and hardness measurement. After correcting machine compliance of the curves in Fig. 11, we calculate the coefficient C of each curve, and then evaluate the residual stress on each position via the method shown in Sec. III. C.

By applying Eq. (8) to the experimental load–depth data, C and $h_g + h_i$ are calculated. Here, not only h_g but also initial penetration depth h_i values are quite similar for unstressed and stressed load–depth data, therefore their $h_g + h_i$ values should also be similar to each other. Because of experimental errors, however, they can have different values and make a huge error of estimated residual stress. In the experiment, we assumed $h_g + h_i$ values to be constant regardless of magnitude of residual stress, and calculated C values only of stressed load–depth curves using $h_g + h_i$ value obtained from unstressed load–depth curve. We then estimated C value of each curve under virtual equi-biaxial residual stress state using Eq. (13), and calculated uniaxial residual stress substituting the C value and tensile material properties into Eq. (14). Simultaneously, we measured the residual stresses on both sides into which we converted strain values measured by strain gauges, and then calculated linearly interpolated residual stresses of the indented positions.

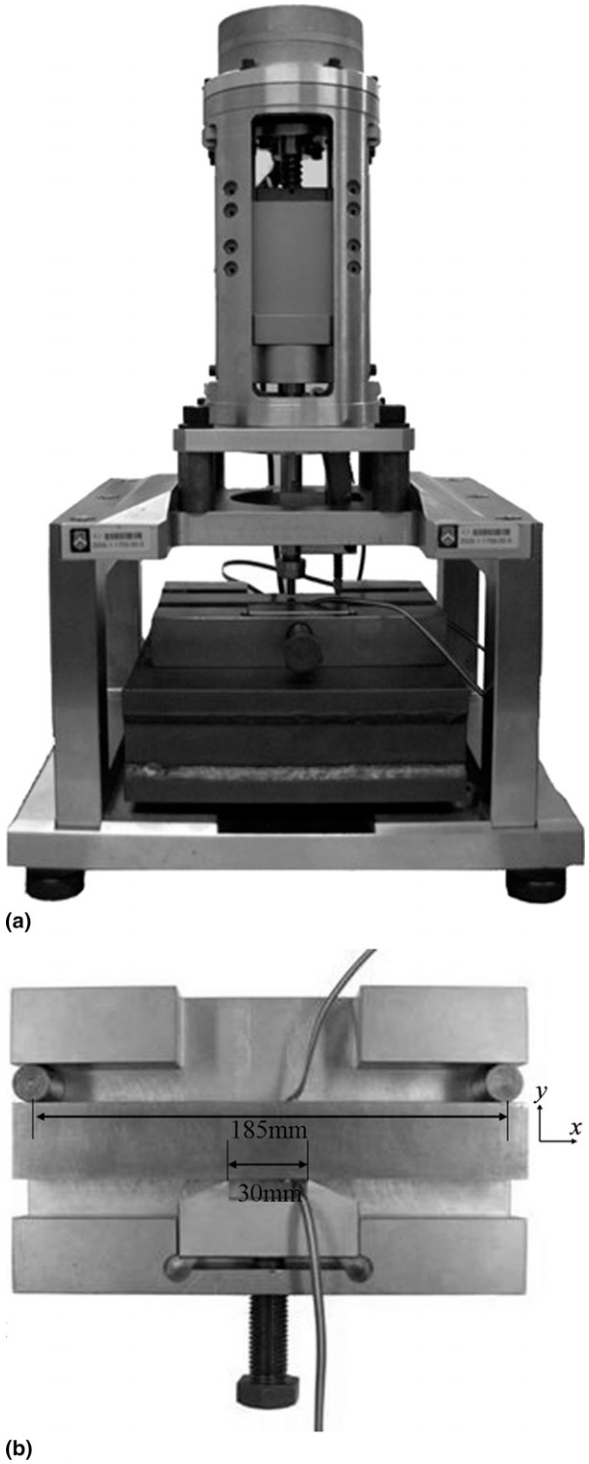

FIG. 10. (a) Configuration of indentation system DKTT-3000 and (b) four-point bending jig (top view).

The residual stresses calculated by our method are compared with those by strain gauges in Table III and Fig. 12, which shows that we can well estimate residual stress using indentation tests within the ±20 MPa range.

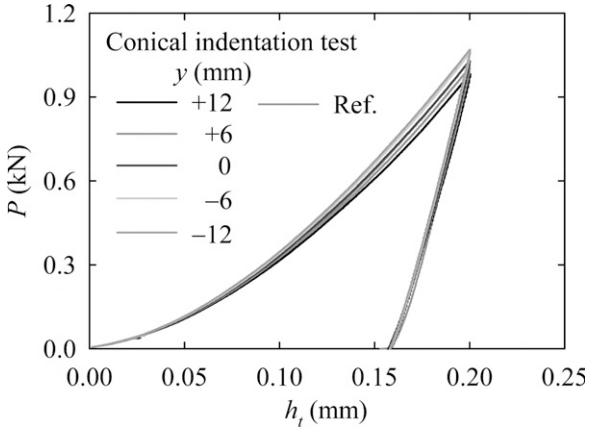

FIG. 11. Load–depth curves obtained from indentation tests (2nd column).

TABLE III. Comparison of uniaxial residual stresses obtained from beam theory, strain gauge, and indentation.

	Strain gauge		Indention (σ_{R1})		
y (mm)	Strain ($\mu\varepsilon$)	σ_S (MPa)	1st column	2nd column	3rd column
+12	+713	+143	+163	+135	+138
+6	+364	+73	+100	+73	+78
0	+16	+3	+12	−3	−2
−6	−333	−67	−68	−85	−58
−12	−682	−137	−175	−150	−158

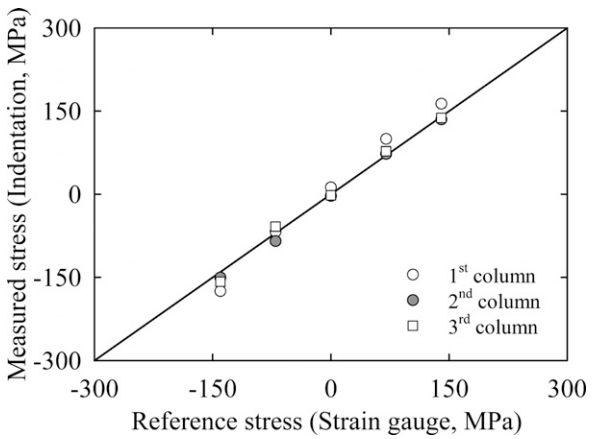

FIG. 12. Linearly varying uniaxial residual stresses evaluated from indentation tests and strain gauge.

On the basis of the experiment, we verified the validity of the uniaxial residual stress evaluation method, which is extended from the elastic biaxial residual stress evaluation method, and hence we expect the biaxial residual stress evaluation method to be also valid. Especially, in the case where the material properties can be known in advance, this method is useful to measure elastic residual stresses because we do not need to measure contact area, tip radius initial penetration depth.

V. CONCLUDING REMARKS

From FE analyses of conical indentation tests, we investigated the relationships between indentation parameters and residual stresses. Hardness depends on the magnitude and sign of residual stress and material properties, while some prior indentation studies reported that hardness is unaffected by residual stress. Of course, there are some studies that showed the hardness dependency on residual stress, but they also did not explain the reason and phenomenon well. Thus, in this work, we analyzed the relation between hardness and residual stress based on finite element analysis and the average indentation depth concept, and from this, we laid out a logical basis for the reason that hardness can depend on residual stress.

On the basis of this observation, we suggested two indentation methodologies to estimate elastic/plastic residual stress via finite element analysis. Using contact area and plastic indentation depth, we first suggested a method for evaluation of elastic/plastic equi-biaxial residual stresses. Then, using tensile material properties (i.e., elastic modulus, yield strength, and strain-hardening exponent), we suggested another method for evaluation of elastic equi-biaxial residual stresses regardless of indenter tip rounding. The second method is practical as it is unnecessary to know the contact area, measurement of which makes indentation tests quite impractical. Because the method reduces measuring errors caused by friction and tip-radius effect, it substantially enhances the accuracy than prior methods. We also suggested a new method to evaluate general biaxial residual stress that was extended from the equi-biaxial residual stress evaluation method. Finally, we measured 4-point linearly varied elastic bending stresses via conical indentation tests, and confirmed that the suggested method is useful and reliable for the evaluation of biaxial residual stress.

ACKNOWLEDGMENT

This work was supported by the National Research Foundation of Korea (NRF) grant funded by the Korea government (MEST) (No. 2007-0052795).

REFERENCES

1. S. Suresh and A.E. Giannakopoulos: A new method for estimating residual stresses by instrumented sharp indentation. *Acta Mater.* **46,** 5755 (1998).
2. S. Carlsson and P.L. Larsson: On the determination of residual stress and strain fields by sharp indentation testing. Part I: Theoretical and numerical analysis. *Acta Mater.* **49,** 2179 (2001).
3. T.Y. Tsui, W.C. Oliver, and G.M. Pharr: Influences of stress on the measurement of mechanical properties using nanoindentation: Part I. Experimental studies in an aluminum alloy. *J. Mater. Res.* **11,** 752 (1996).

4. A. Bolshakov, W.C. Oliver, and G.M. Pharr: Influences of stress on the measurement of mechanical properties using nanoindentation: Part II. Finite element simulations. *J. Mater. Res.* **11,** 760 (1996).
5. Y-H. Lee and D. Kwon: Estimation of biaxial surface stress by instrumented indentation with sharp indenters. *Acta Mater.* **52,** 1155 (2004).
6. E. Atar, C. Sarioglu, U. Demirler, E.S. Kayali, and H. Cimenoglu: Residual stress estimation of ceramic thin films by x-ray diffraction and indentation techniques. *Scr. Mater.* **48,** 1331 (2003).
7. Z.H. Xu and X. Li: Influence of equi-biaxial residual stress on unloading behaviour of nanoindentation. *Acta Mater.* **53,** 1913 (2005).
8. X. Chen, J. Yan, and A.M. Karlsson: On the determination of residual stress and mechanical properties by indentation. *Mater. Sci. Eng., A* **416,** 139 (2006).
9. J.H. Lee, H. Lee, and D.H. Kim: A numerical approach to evaluation of elastic modulus using conical indenter with finite tip-radius. *J. Mater. Res.* **23,** 2528 (2008).
10. ABAQUS: *ABAQUS User Manual* (Simulia Co., Providence, RI, 2008).
11. H. Lee, J.H. Lee, and G.M. Pharr: A numerical approach to spherical indentation technique for material property evaluation. *J. Mech. Phys. Solids* **53,** 2037 (2005).
12. M. Dao, N. Chollacoop, K.J. Van Vliet, T.A. Venkatesh, and S. Suresh: Computational modeling of the forward and reverse problems in instrumented sharp indentation. *Acta Mater.* **49,** 3899 (2001).
13. J.R. Rice and G.F. Rosengren: Plane strain deformation near a crack-tip in a power law hardening material. *J. Mech. Phys. Solids* **16,** 1 (1968).
14. B. Taljat, T. Zacharia, and F. Kosel: New analytical procedure to determine stress–strain curve from spherical indentation data. *Int. J. Solids Struct.* **35,** 4411 (1998).
15. J.H. Lee, T. Kim, and H. Lee: A study on robust indentation techniques to evaluate elastic–plastic properties of metals. *Int. J. Solids Struct.* **47,** 647 (2010).
16. A.C. Fischer-Cripps: A review of analysis methods for sub-micron indentation testing. *Vacuum* **58,** 569 (2000).
17. J.R. Barber and D.A. Billings: An approximate solution for the contact area and elastic compliance of a smooth punch of arbitrary shape. *Int. J. Mech. Sci.* **32,** 991 (1990).
18. Z.H. Xu and X. Li: Effects of indenter geometry and material properties on the correction factor of Sneddon's relationship for nanoindentation of elastic and elastic–plastic materials. *Acta Mater.* **56,** 1399 (2008).
19. S. Shim, W.C. Oliver, and G.M. Pharr: A comparison of 3D finite element simulations for Berkovich and conical indentation of fused silica. *Int. J. Surf. Sci. Eng.* **1,** 259 (2007).
20. J.H. Lee, Y.F. Gao, and G.M. Pharr: An approach to analysis of indentation data using three-sided and conical indenters. (In preparation).
21. H.C. Hyun, J.H. Lee, and H. Lee: Mathematical expressions for stress–strain curve of metallic material. *Trans. KSME* **32,** 21 (2008).

APPENDIX: THE COEFFICIENT VALUES OF REGRESSION FUNCTIONS OF EQS. (10)–(11)

TABLE AI. Coefficients of Eq. (10).

	$i=0$			
	$k=0$	$k=1$	$k=2$	$k=3$
$j=0$	2.143e-1	−7.796e+1	1.182e+4	−5.679e+5
$j=1$	−1.241e+0	5.776e+2	−8.732e+4	4.222e+6
$j=2$	3.654e+0	−1.765e+3	2.722e+5	−1.332e+7
$j=3$	−5.172e+0	2.538e+3	−3.978e+5	1.973e+7
$j=4$	2.780e+0	−1.359e+3	2.177e+5	−1.091e+7
	$i=1$			
	$k=0$	$k=1$	$k=2$	$k=3$
$j=0$	−9.067e-3	4.348e+0	−6.879e+2	3.403e+4
$j=1$	8.136e-2	−4.169e+1	6.677e+3	−3.339e+5
$j=2$	−2.789e-1	1.485e+2	−2.425e+4	1.229e+6
$j=3$	4.217e-1	−2.304e+2	3.826e+4	−1.961e+6
$j=4$	−2.337e-1	1.300e+2	−2.190e+4	1.131e+6

TABLE AII. Coefficients of Eq. (11).

	$j=0$	$j=1$	$j=2$	$j=3$
$i=0$	−4.300e-3	1.116e+2	−6.630e+3	2.275e+5
$i=1$	3.590e-1	6.039e+1	−2.043e+3	−6.216e+4
$i=2$	−6.629e-1	6.654e+2	−1.021e+5	4.843e+6
$i=3$	2.339e+0	−8.162e+2	1.075e+5	−4.849e+6